Energy 224 (2021) 120134

Contents lists available at ScienceDirect

Energy

journal homepage: www.elsevier.com/locate/energy

Performance assessment of a novel biomass-based solid oxide fuel cell power generation cycle; Economic analysis and optimization

Cai Cheng [a], Jacob Cherian [b], Muhammad Safdar Sial [c,*], Umer Zaman [d], Hosein Niroumandi [e]

[a] Economics and Management School, Wuhan University, Wuhan, Hubei, 430072, China
[b] College of Business, Abu Dhabi University, Abu Dhabi, United Arab Emirates
[c] Department of Management Sciences, COMSATS University Islamabad (CUI), Islamabad, Pakistan
[d] Endicott College of International Studies, Woosong University, Daejeon, 34606, South Korea
[e] Young Researches and Elite Club, Bonab Branch, Islamic Azad University, Bonab, Iran

A R T I C L E I N F O

Article history:
Received 4 June 2020
Received in revised form
31 January 2021
Accepted 14 February 2021
Available online 17 February 2021

Keywords:
Biomass-based solid oxide fuel cell
Economic analysis
Levelized total emission
Net present value
Payback period

A B S T R A C T

In the present work, a novel combined system based on the biomass-based solid oxide fuel cell and gas turbine system combined with the organic flash cycle is regarded for power generation aim. The main objective of this work is to investigate the feasibility of the proposed system from the economic and environmental viewpoints. The optimum performance of all optimization scenarios is found by applying the multi-objective particle swarm optimization algorithm and using the technique for order of preference by similarity to ideal solution (TOPSIS) method. Regarding the obtained results, for fuel cost of 6$\$/GJ$ and electricity price of 0.10$\$/kWh$, the total net present value at the end of plant lifetime is 9.8×10^5 \$ and the payback period is 4.25 years, which means that the plant is feasible for construction from the economic perspective. Also, the simulation results indicate that the proposed hybrid system can yield to the energy and exergy efficiencies of 49.37% and 42.50%, respectively. Also, the net output electrical power and is obtained 425.39kW. Moreover, the final optimum solution selected by the decision-making method is obtained by $\eta_{II} = 47.12\%$, $LTE = 23.24\ t/MWh$, and $c_{p,tot} = 5.50\ \$/GJ$.

1. Introduction

As energy demands continue to increase, researchers continue to seek alternative energy resources to generate electricity and improve conventional methods to maximize efficiency. A greater reliance on electricity generated from renewable energy sources such as biomass and hydrogen fuel will become essential to meet global energy demands. Therefore, biomass utilization in renewable energy systems has a high importance in future renewable energy sources. Biomass is regarded as a feasible route to realizing a sustainable future since biomass is a carbon-neutral energy source and can reduce our dependence on fossil fuels [1].

1.1. Biomass gasification

Gasification is one of the most effective methods for using the latent energy of biomass. During this process, decomposition is made by heating, and the final potential efficiency of this method is higher than combustion [2]. Gasifiers are designed and produced in various capacities and sizes for different aims. Gasification processes are categorized into three different classes based on the mass transfer mechanism and reactor design, including fixed-bed, fluidized-bed, and the continuous laminar flow. Gasification agent can be steam or air for performing the biomass gasification in the auto-thermal process. Air gasification is an exothermic process, while steam gasification is an endothermic process that requires an external heat source [3].

Several methods are proposed for utilizing different types of biomass in energy systems [4]. One of these methods is to burn biomass to supply the energy of the boiler in power and heat generation systems. The utilization of biomass in the gasification reactor is an efficient approach that can produce a mixture of flammable and high-quality gases that can be applied in high-efficiency plants [5]. Shayan et al. [6] studied hydrogen production from biomass gasification employing different agents and

* Corresponding author.
E-mail address: safdarsial@comsats.edu.pk (M.S. Sial).

https://doi.org/10.1016/j.energy.2021.120134
0360-5442/

Nomenclature

Symbols

A_c	Active surface area of cell [m^2]
c	Cost per exergy unit [$/GJ]
$\dot{C}$	Cost rate [$/h]
CRF	Capital recovery ratio [−]
$\dot{E}$	exergy rate [kW]
F	Faraday constant [C/mol]
f_k	Exergoeconomic metric [−]
G	Gibbs free energy [kJ]
HHV	Higher heating value [MJ/kg]
h	specific enthalpy [kJ/kg]
interest rate [−]	
j	Current density (A/m^2)
K	Equilibrium constant [−]
L	Thickness of SOFC layers, [mm]
LHV	Lower heating value [kJ/kg]
LTE	Levelized total emission [t/MWh]
M	Molar weight [kg/kmol]
$\dot{m}$	mass flow rate [kg/s]
$\dot{n}$	molar rate [mol/s]
n_e	Number of electrons participating in the reaction [−]
n	Lifetime [years]
N_c	Number of cells in the stack [−]
P	Pressure [kPa]
PR	Pressure Ratio [−]
p_{H_2O}	H_2O partial pressure [kPa]
p_{H_2}	H_2 partial pressure [kPa]
p_{O_2}	O_2 partial pressure [kPa]
$\dot{Q}$	Heat transfer rate[kW]
$\overline{R}$	Universal gas constant [J/mol·K]
R_{AR}	Recycling ratio of anode [−]
R_{CR}	Recycling ratio of cathode [−]
s	specific entropy [kJ/kg·K]
T	temperature [°C]
U	Overall heat transfer coefficient [W/m^2·K]
U_f	Fuel utilization factor [−]
V_c	Cell voltage [V]
$\dot{W}$	Electrical power [kW]
w	Moisture content [kmol/kmol]
x_r	extent of steam-methane reforming reaction [mol/ s]
y_r	extent of water gas shift reaction [mol/s]
z_r	extent of overall electrochemical reaction [mol/ s]
Z	Investment cost [$]
$\dot{Z}$	Investment cost rate [$/h]

Subscripts and superscripts

AB	Afterburner
AC	Air compressor
act	activation
conc	concentration
D	destruction
eff	Effective
en	Energy
ex	Exergy
f	Formation
F	Fuel
FC	Fuel compressor
GT	Gas turbine
g	Gasification
in	Inlet
inv	DC to AC inverter
mix	Mixer
N	Nernst
net	net value
ohm	Ohmic
out	Outlet
P	product
ph	Physical
pum	Pump
TPB	Triple phase boundary
Tur	Turbine
tot	Total value
th	Thermal
1, 2, …	cycle locations
0	dead state

Greek Symbols

ε	effectiveness
η	efficiency
Δ	difference
τ	Annual number of hours

Abbreviations

EES	Engineering Equation Solver
GT	Gas Turbine
NPV	Net Present Value
OFC	Organic Flash Cycle
PSO	Particle Swarm Optimizer
PP	Payback Period
SOFC	Solid Oxide Fuel Cell
TOPSIS	Technique for Order of Preference by Similarity to Ideal Solution
WHR	Waste Heat Recovery

compared theoretically, from the energy and exergy viewpoints. Based on their obtained results, the highest energy efficiency value is obtained for air gasification, while the highest exergy efficiency is obtained for steam gasification. Also, they resulted that the increment of the gasification temperature leads to a flat curve for hydrogen concentration in the case of steam gasification.

The quality of the produced gas through the gasification process can be affected by several parameters, including the gasification temperature, biomass moisture, type of gasification agent, and mass flow rate of gasification agent. Several studies are conducted on different gasification agents, including utilization of the air, oxygen, mixture of air and steam, and pure steam. An experimental study is presented by Sharma et al. [7]. For different equivalence ratios in the downdraft gasifier. They reported the effects of the steam to biomass ratio and as well as effects of direct insertion of the steam to the reduction zone on the output gas composition. A thermodynamic model is developed by Balu et al. [8] for high-temperature wood gasification with steam as the gasification agent for the prediction of the syngas compositions and solid carbon deposition. They obtained an optimum range for the steam to biomass molar ratio. Schuster et al. [9] presented a model for steam gasification through thermodynamic equilibrium equations. They carried out a sensitivity study and concluded that two factors have a considerable effect on gasification chemical efficiency, including gasification temperature and the oxygen content in the fuel. Meantime, several studies have also been done on syngas utilization in high-efficiency and sustainable energy plants. For instance, an analysis is performed by Bartela et al. [10] from the economic aspect for utilization of the Stirling engine in a combined system based on biomass gasification. Based on their obtained results, the gasification-based system with a Stirling engine is more justified for a higher ratio of the sale price of electricity to the sale price of heat.

1.2. Biomass gasification-based solid oxide fuel cell

Fuel cells, such as solid oxide fuel cells (SOFCs), are efficient systems that can directly convert chemical substrates into electricity. The most important advantages of the fuel cells are vibration-free and noise-free operation, high efficiency, and low environmental contamination [11]. Accordingly, many researchers devised and analyzed integrated energy systems consisting of a biomass-based SOFC. Li et al. [12] performed a techno-economic analysis on tubular SOFC, where N_2O is considered as the oxidant instead of air. They revealed that the power density is increased about 50% where a considerable decrement in greenhouse gas emissions was observed. Doherty et al. [13] evaluated the feasibility of an integrated biomass gasification SOFC system. Based on their results, the steam to carbon ratio and steam content of the biomass should be as low as possible, while hot syngas cleaning is preferred. Tan et al. [14] proposed an integrated biomass-based SOFC system consisting of gas expanders and a Kalina system. The results showed that total exergy destruction might be 397 kW for the base condition, and the hybrid system's efficiency would be 64.20%. Panopoulos [15] designed and analyzed an integrated biomass gasification-SOFC system where steam is utilized as the gasification agent. They obtained the values of 36% and 32% for energy and exergy efficiencies, where the current density is considered 2500 A/m^2. Perna et al. [16] experimentally investigated the biomass-based SOFC system, and they resulted that at the best operating condition, the power output may be 262 kW.

1.3. Waste heat recovery of solid oxide fuel cell stack

For improving the efficiency of the thermodynamic systems and decline the pollutants emission to the environment and decline the fuel utilization, waste heat recovery (WHR) approaches can be employed. The exhaust off-gases of the SOFC-GT contain a higher level of waste energy, which can drive the bottoming cycles within a waste heat recovery unit. Various WHR methods are recommended to reuse the waste heat of the exhaust gases [17]. Some researchers proposed new configurations for exploiting the exhaust gases of SOFCs in other systems, e.g., gas turbine (GT), Stirling engine, organic Rankine cycle, and Kalina cycle to provide further power from the waste heat of the exhaust gases [18]. Ranjbar et al. [19] studied and compared two configurations consisting of a SOFC/Kalina and a SOFC/organic Rankine cycle for waste heat recovery of the SOFC unit. They concluded that the combined system's efficiency could be increased by about 33% compared to the stand-alone SOFC unit. Oryshchyn et al. [20] evaluated fuel consumption in a hybrid system of a gas turbine and an SOFC. The results revealed that the maximum efficiency of the system might be 75.60%, and for minimized degradation of SOFC, the efficiency decreases by about 7%. Ahmadi et al. [21] proposed and analyzed two different configurations of SOFC-driven combined systems for power and heating production. They evaluated the proposed systems from the energy and exergy viewpoints. The results indicated that the energy efficiency could be enhanced by 60.05% compared to the stand-alone SOFC system by utilization of solid oxide fuel cell-Absorption refrigeration cycle-Domestic hot water (SOFC-APC-DHW) configuration. Haseli et al. [22] analyzed an integrated system consisting of a SOFC and GT from the energy and exergy viewpoints. The results revealed that by raising the gas turbine inlet temperature, the energy efficiency of the system decreases but power output increases.

1.4. Organic flash cycle

One of the main challenges in cycles using organic fluids as the working fluid is the high exergy destruction (chiefly in evaporators), where the temperature mismatch of hot flow and cold flow is the main reason for the exergy dissipation. Some methods are presented to reduce the exergy destruction rate, such as the application of the transcritical, trilateral, and two-stage systems and utilization of the zeotropic mixture as the working fluid. Organic flash cycles (OFCs) are another solution to avoid the pinch limitation of the conventional ORCs in which the working fluid becomes a saturated liquid in the heat absorber during the heat addition process; the saturated working is then flashed to produce a two-phase mixture. Ho et al. [23] studied the power generation capacity of the organic flash cycle compared to the basic ORC system. They resulted that the OFC power generation capacity is comparable to the power generation capacity of the ORC unit. A comparison is presented by Lee et al. [24] from the thermodynamic viewpoint for three different configurations, including the basic OFC, OFC with a two-phase expander, and an ORC cycle. Regarding their results, the OFC system can efficiently generate higher power from low-temperature heat sources compared to the other two systems. Hedelu and Boyaghchi [25] proposed four novel configurations of two-stage expander organic flash cycles (EOFCs) based on the ejector. They analyzed the devised systems from the exergy, exergoeconomic, and exergoenvironmental perspectives. A performance comparison revealed that the net output power, energy efficiency, and exergy efficiency are improved by 16.83%, 13.05%, and 10.99%, receptively, in EF1-EOFC, E-EOFC, and DE-EOFC relative to the base EOFC. Wu et al. [26] proposed a novel combined cooling and power (CCP) system consisting of an OFC cycle and an ammonia-water absorption refrigeration cycle. They also studied the effect of eight different organic flash cycle working fluids. Among the eight considered organic fluids, the n-Nonane brings the lowest total product unit cost and highest exergy efficiency.

1.5. Main contributions and novelties

To the best of the authors' knowledge and based on the reviewed literature in the above paragraphs, many investigations have been devoted to devising and studying new hybrid systems based on the SOFC system; however, there is no study on biomass-based SOFC integrated with a GT and OFC. Accordingly, a novel configuration of biomass gasification and SOFC/GT/OFC is devised for power generation purposes. Exploiting the organic flash cycle for the waste heat recovery of the SOFC is another novelty of the devised plant for decreasing the environmental impacts and increasing power generation capacity. The main objective of this work is to investigate the feasibility of the proposed system from thermodynamic, economic, and environmental viewpoints. Hence, the proposed power generation plant is analyzed thoroughly from the energy, exergy, exergoeconomic, and environmental (4E) viewpoints. Also, a multi-objective particle swarm optimizer is applied for the proposed system in which air is considered as the gasifier agent to maximize the exergy efficiency and minimize total product cost and Levelized total emission at the same time.

The main objectives and novelties of the present work can be summarized as:

- To devise a novel configuration for power generation aims, employing Gasifier, SOFC, gas turbine, and OFC systems.
- To study the energy, exergy, environmental, and economic aspects of the devised system.
- To decrease the environmental impacts and increase the power generation capacity by exploiting the waste energy of the topping system in the OFC system.
- To investigate the feasibility of the proposed system using net present value and payback period concepts.
- To obtain the optimum solution points as Pareto frontiers and calculate the most favorable solution points from various perspectives.
- To study the scatter distribution of the decision variables and determine the best operating range of the decision variables.

2. System description and presumptions

The schematic diagram of the proposed power generation plant is presented in Fig. 1. A downdraft gasifier is employed to prepare the syngas for the SOFC, and a GT and OFC is selected to exploit the waste heat of the SOFC. Initially, the air compressor is used to compress the ambient air (state 1) into the heat exchanger (state 2). Then, the compressed air is heated up by afterburner output gases (state 3a) and mixed with the recirculated gases of the cathode (state 3b) in the mixer and delivered to the cathode-side channel (state 3). On the other side, biomass is supplied as the fuel into the gasifier (state 5). The high-temperature air heated up in the air preheater by the afterburner exhaust gases is fed as the gasification agent (process 15 to 16). In the gasifier, considering all phenomena and reactions, the produced syngas is blown by the blower into the mixer (process 6 → 7). In the mixer, the recirculated gases of the anode (state 8b) are mixed in the mixer with the syngas, and the output mixed gases are fed into the anode (state 8). Regarding the electrochemical reactions in the SOFC stack, the SOFC stack can generate DC, which can be further converted to AC by inverter. After completing all phenomena in the SOFC stack, part of the un-reacted off-gases in the anode and cathode (states 3b and 8b) are recirculated, and part of off-gases are burnt in the afterburner (states 4a and 9b). Following that, the outlet gases of the afterburner (state 10) pass within an air preheater to heat the input air of the gasifier unit. Subsequently, after heating the air in the air preheater, the off-gases (state 11) pass within the air heat exchanger to heat the inlet air of the cathode. Afterward, the exhaust high-temperature off-gases pass through a gas turbine to improve the power generation capacity (process 12 → 13). Eventually, the exhaust gases of the GT are delivered to the OFC system in the heat exchanger for further electricity generation.

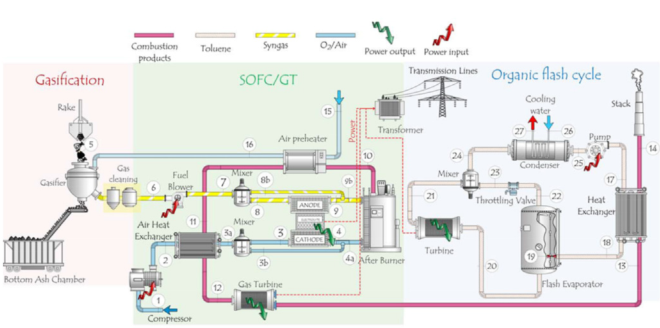

Fig. 1. Schematic of the proposed combined SOFC/GT-OFC system.

On the other hand, the organic flash cycle operates by obtaining the energy from the gas turbine off-gases in the heat exchanger. The OFC detailed layout and the corresponding T-s diagram with Toluene as the working fluid are shown in Fig. 2.

The working process of the OFC cycle is described as follows: after being heated in the heat exchanger to saturated liquid (process 17 → 18), the working fluid undergoes an expansion process in the throttling valve to produce a two-phase flow (process 18 → 19). Following the expansion valve, the two-phase working fluid is divided into two streams; saturated liquid and vapor flow (states 22 and 20). The saturated vapor flow is delivered to the steam turbine to be expanded within the turbine for power generation (process 20 → 21). The saturated flow leaving the flash evaporator throttles in the low-pressure throttling valve (process 22 → 23). Then, the flows leaving the turbine and throttling valve are mixed in the mixer. Subsequently, the working fluid is condensed to a saturated liquid using cooling water in the condenser (process 24 → 25). Ultimately, the saturated liquid is pressurized by the circulating pump to the heat exchanger pressure (state 17) and completes the cycle.

Main assumptions and limitations of this study are as follows [21]:

- The ideal gas assumption is considered for the air, syngas, and flue gases.
- For the simplified analysis, the steady-state condition is assumed for the analyses.
- Kinetic and potential energy changes are neglected.
- Heat loss from the boundary of each component is neglected.
- The contact resistance in the SOFC layers is negligible.

Also, some main input parameters for the steady-state simulation are presented in Table 1.

3. Mathematical modeling of system components

Here, the proposed power generation system is comprehensively analyzed from the energy, exergy, economic, exergoeconomic, and environmental perspectives. The Engineering equation solver (EES) software is used to calculate the corresponding equations based on energy, exergy, and exergoeconomic analyses [27]. EES is a general equation-solving program that can numerically solve thousands of coupled non-linear algebraic and differential equations. A major feature of EES is high accuracy thermodynamic and transport property database that is provided for hundreds of substances in a manner that allows it to be used with the equation solving capability.

3.1. Mass, energy, and exergy analysis

In this subsection, mass, energy, and exergy balance equations are employed for assessment of the suggested cycle as follows [28,29]:

$$\sum_{in} \dot{m} - \sum_{out} \dot{m} = 0 \tag{1}$$

$$\dot{Q} - \dot{W} = \sum \dot{m}_{out} h_{out} - \sum \dot{m}_{in} h_{in} \tag{2}$$

$$\dot{E}_D = \sum \dot{E}_{in} - \sum \dot{E}_{out} \tag{3}$$

Where $\dot{m}$ is the mass flow rate, h denotes the specific enthalpy, $\dot{Q}$ and $\dot{W}$ are the heat transfer rate and mechanical powers, and in and

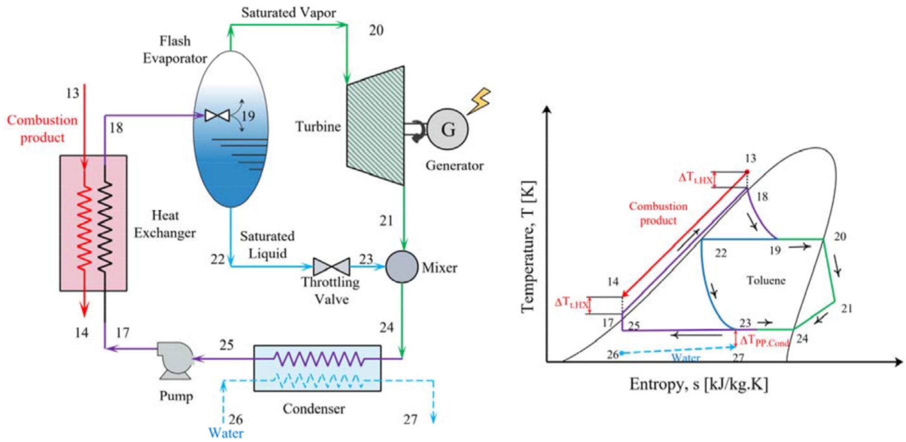

Fig. 2. Demonstrative outline of the organic flash cycle with corresponding T-S diagram.

Table 1
Some of the main input parameters for the steady-state simulation of the devised system.

Parameter	Value	Parameter	Value
$T_g [^\circ C]$	600	$A_a [m^2]$	0.01
$T_{inlet,air} [^\circ C]$	25	$T_{SOFC,inlet} [^\circ C]$	726.85
$T_{inlet,biomass} [^\circ C]$	25	$j_{anode} [A/m^2]$	6500
$\eta_{is,GT} [\%]$	80	$j_{cathode} [A/m^2]$	2500
$T_{cond} [^\circ C]$	15	$L_{anode} [mm]$	0.5
$T_{18} [^\circ C]$	286	$L_{cathode} [mm]$	0.05
$\Delta T_{PP,H.X.} [^\circ C]$	20	$L_{electrolyte} [mm]$	0.01
$T_{19} [^\circ C]$	230	$L_{interconnect} [mm]$	3
$\eta_{is,ST} [\%]$	85	$N_{cells} [-]$	11000
$\eta_{is,Pump} [\%]$	85	$\eta_{FC} = \eta_{AC} [\%]$	85
$j [A/m^2]$	5000	$R_{CR} [-]$	0.4
$U_f [-]$	0.85	$PR_{AC} [-]$	1.21
$R_{AR} [-]$	0.4	$PR_{FC} [-]$	1.21
$\Delta T_{stack} [^\circ C]$	100	$\eta_{inv} [\%]$	95

out refers to the input and output streams in each component. Also, the exergy rate includes chemical and physical exergy, and $\dot{E}_D$ denotes for exergy destruction rate. Exergy balance equations as well as exergetic efficiency for different components in the system is presented in Table 2.

3.1.1. Gasification analysis

In this paper, the downdraft gasifier is considered to supply the required fuel of the SOFC stack. The equilibrium condition is considered regarding the thermodynamic equilibrium for all reactions. Relevant reactions to the gasification process are presented, in which air is considered as the gasification agent [30,31]:

$$\text{Boudouard reaction } C + CO_2 \leftrightarrow 2CO;\ \Delta H = +172\ \text{MJ/kmol} \tag{4}$$

$$\text{Water-gas heterogeneous reaction } C + H_2O \leftrightarrow CO + H_2;\ \Delta H = +131\ \text{MJ/kmol} \tag{5}$$

$$\text{Methane formation reaction } C + 2H_2 \leftrightarrow CH_4;\ \Delta H = -75\ \text{MJ/kmol} \tag{6}$$

$$\text{Water-gas shift reaction } CO + H_2O \leftrightarrow CO_2 + H_2;\ \Delta H = -41\ \text{MJ/kmol} \tag{7}$$

Additionally, the global gasification reaction for the air as the gasification agent is [32]:

$$CH_aO_bN_c + wH_2O + n_{air}[O_2 + 3.76N_2] \leftrightarrow n_{H_2}H_2 + n_{CO}CO + n_{CO_2}CO_2 + n_{H_2O}H_2O + n_{CH_4}CH_4 + n_{N_2}N_2 \tag{8}$$

Where $CH_aO_bN_c$ is the biomass fuel, w is the moisture content of biomass, n_{air} indicates the kmol of the gasification agent. Mass balance for Carbon, Oxygen, Hydrogen, and Nitrogen is implemented to determine the relevant coefficients. The ultimate analysis of biomass is considered as: $50\%\ C; 6\%\ H; 0\%\ N; 0\%\ S; 44\%\ O; 0\%\ \text{Ash, and HHV} = 19.97\ \text{MJ/kg}$.

The equilibrium condition is assumed for the reactions. In this regard, the equilibrium constants for methane formation and water-gas shift reactions are presented as [30]:

$$K_1 = \frac{n_{CH_4}}{n_{H_2}^2}\left(\frac{P/P_0}{n_{tot}}\right)^{-1} \tag{9}$$

$$K_2 = \frac{n_{H_2}n_{CO_2}}{n_{CO}n_{H_2O}}\left(\frac{P/P_0}{n_{tot}}\right)^{0} \tag{10}$$

Accordingly, the equilibrium constants should be computed using Gibbs function [33]:

$$-\frac{\Delta G_1^0}{\overline{R}T_g} = \ln K_1 \tag{11}$$

$$-\frac{\Delta G_2^0}{\overline{R}T_g} = \ln K_2 \tag{12}$$

Where T_g denotes the gasification temperature based on Kelvin.

$$-\Delta G_1^0 = \left(\overline{h}_{CH_4} - T_g\overline{s}^0_{CH_4}\right) - 2\left(\overline{h}_{H_2} - T_g\overline{s}^0_{H_2}\right) \tag{13}$$

$$-\Delta G_2^0 = \left(\overline{h}_{CO_2} - T_g\overline{s}^0_{CO_2}\right) + \left(\overline{h}_{H_2} - T_g\overline{s}^0_{H_2}\right) - \left(\overline{h}_{CO} - T_g\overline{s}^0_{CO}\right) - \left(\overline{h}_{H_2O} - T_g\overline{s}^0_{H_2O}\right) \tag{14}$$

Finally, the energy balance is used for the gasification system for

Table 2
Exergy balance equations as well as exergetic efficiency for different components in the system.

Component	Exergy balance	Exergy efficiency
Gasifier	$\dot{E}_{D,G} = \dot{E}_5 + \dot{E}_{16} - \dot{E}_6$	$\eta_{II,G} = \dot{E}_6/(\dot{E}_5 + \dot{E}_{16})$
Fuel blower	$\dot{E}_{D,FC} = \dot{W}_{FC}-(\dot{E}_7 - \dot{E}_6)$	$\eta_{II,FC} = (\dot{E}_7 - \dot{E}_6)/\dot{W}_{FC}$
Air Heat exchanger	$\dot{E}_{D,AHX} = \dot{E}_{11} - \dot{E}_{12} - (\dot{E}_{3a} - \dot{E}_2)$	$\eta_{II,AHX} = (\dot{E}_{3a} - \dot{E}_2)/(\dot{E}_{11} - \dot{E}_{12})$
Anode mixer	$\dot{E}_{D,AM} = \dot{E}_7 + \dot{E}_{8b} - \dot{E}_8$	$\eta_{II,AM} = \dot{E}_8/(\dot{E}_7 + \dot{E}_{8b})$
Cathode mixer	$\dot{E}_{D,CM} = \dot{E}_{3b} + \dot{E}_{3a} - \dot{E}_3$	$\eta_{II,CM} = \dot{E}_3/(\dot{E}_{3b} + \dot{E}_{3a})$
SOFC Stack	$\dot{E}_{D,SOFC} = \dot{E}_3 + \dot{E}_8 - (\dot{E}_4 + \dot{E}_9) - W_{SOFC,stack,DC}$	$\eta_{II,SOFC,stack} = (\dot{E}_4 + \dot{E}_9 - W_{SOFC,stack,DC})/(\dot{E}_3 + \dot{E}_8)$
Afterburner	$\dot{E}_{D,AB} = \dot{E}_{4a} + \dot{E}_{9b} - \dot{E}_{11}$	$\eta_{II,AB} = \dot{E}_{11}/(\dot{E}_{4a} + \dot{E}_{9b})$
Inverter	$\dot{E}_{D,INV} = \dot{W}_{SOFC,stack,DC} - \dot{W}_{SOFC,stack,AC}$	$\eta_{II,INV} = \dot{W}_{SOFC,stack,AC}/\dot{W}_{SOFC,stack,DC}$
Air preheater	$\dot{E}_{D,Ap} = \dot{E}_{10} - \dot{E}_{11} - (\dot{E}_{16} - \dot{E}_{15})$	$\eta_{II,Ap} = (\dot{E}_{16} - \dot{E}_{15})/(\dot{E}_{10} - \dot{E}_{11})$
Gas turbine	$\dot{E}_{D,GT} = \dot{E}_{12} - (\dot{E}_{13} + \dot{W}_{GT})$	$\eta_{II,GT} = (\dot{E}_{13} + \dot{W}_{GT})/\dot{E}_{12}$
Air compressor	$\dot{E}_{D,AC} = \dot{W}_{AC} - (\dot{E}_2 - \dot{E}_1)$	$\eta_{II,AC} = (\dot{E}_2 - \dot{E}_1)/\dot{W}_{AC}$
Heat exchanger	$\dot{E}_{D,HX} = \dot{E}_{13} - \dot{E}_{14} - (\dot{E}_{18} - \dot{E}_{17})$	$\eta_{II,HX} = (\dot{E}_{18} - \dot{E}_{17})/(\dot{E}_{13} - \dot{E}_{14})$
Flash evaporator	$\dot{E}_{D,Eva} = \dot{E}_{18} - (\dot{E}_{20} + \dot{E}_{22})$	$\eta_{II,Eva} = (\dot{E}_{20} + \dot{E}_{22})/\dot{E}_{18}$
Turbine	$\dot{E}_{D,T} = \dot{E}_{20} - (\dot{E}_{21} + \dot{W}_{ST})$	$\eta_{II,T} = (\dot{E}_{21} + \dot{W}_{ST})/\dot{E}_{20}$
Mixer	$\dot{E}_{D,M} = \dot{E}_{21} + \dot{E}_{23} - \dot{E}_{24}$	$\eta_{II,M} = \dot{E}_{24}/(\dot{E}_{21} + \dot{E}_{23})$
Throttling valve	$\dot{E}_{D,th.v} = \dot{E}_{23} - \dot{E}_{22}$	$\eta_{II,th.v} = \dot{E}_{22}/\dot{E}_{23}$
Condenser	$\dot{E}_{D,Cond} = (\dot{E}_{24} + \dot{E}_{25}) - (\dot{E}_{27} - \dot{E}_{26})$	$\eta_{II,Cond} = (\dot{E}_{27} - \dot{E}_{26})/(\dot{E}_{24} + \dot{E}_{25})$
Pump	$\dot{E}_{D,pm} = \dot{W}_{pm} - (\dot{E}_{17} - \dot{E}_{25})$	$\eta_{II,pm} = (\dot{E}_{17} - \dot{E}_{25})/\dot{W}_{pm}$

obtaining the air to fuel ratio.

$$\bar{h}^0_{f,biomass} + w \times \bar{h}^0_{f,H_2O} = n_{H_2}\left(\bar{h}^0_{f,H_2} + \Delta\bar{h}_{H_2}\right) + n_{CO}\left(\bar{h}^0_{f,CO} + \Delta\bar{h}_{CO}\right) + n_{CO_2}\left(\bar{h}^0_{f,CO_2} + \Delta\bar{h}_{CO_2}\right) + n_{H_2O}\left(\bar{h}^0_{f,H_2O} + \Delta\bar{h}_{H_2O}\right) + n_{CH_4}\left(\bar{h}^0_{f,CH_4} + \Delta\bar{h}_{CH_4}\right) + n_{N_2}\left(\bar{h}^0_{f,N_2} + \Delta\bar{h}_{N_2}\right) \quad (15)$$

3.1.2. Solid oxide fuel cell

Solid oxide fuel cell is an electrochemical device which converts the chemical energy to electricity directly. Different range of fuels can be employed to drive the SOFC. In this work, the product syngas of the gasifier is used to fed into stack. The related reforming and shifting reactions of the SOFC stack are respectively defined as [16]:

$$\text{Reforming reaction } x_r \rightarrow CH_4 + H_2O \rightarrow CO + 3H_2 \quad (16)$$

$$\text{Shifting reaction} y_r \rightarrow CO + H_2O \rightarrow CO_2 + H_2 \quad (17)$$

In addition, the overall reaction is presented by:

$$\text{Overall reaction } z_r \rightarrow H_2 + 0.5O_2 \rightarrow H_2O \quad (18)$$

Regarding performed works in the literature, H_2 dominates over CO from the charge transfer viewpoint. Main part of the current is generated by H_2 oxidation and effect of the CO oxidation is negligible [34]. Therefore, based on an acceptable approximation, it is assumed that CO only contributes in the water-gas-shift reaction. Accordingly, the equilibrium constants of the reforming reaction and shifting reactions can be determined by Ref. [34]:

$$\ln K_R = -\frac{\Delta\bar{g}^0_R}{\bar{R}T_{FC,e}} = \ln\left[\left(\frac{\left[\dot{n}_{CO} + x_r - y_r\right] \times \left[\dot{n}_{H_2} + 3x_r + y_r - z_r\right]}{\left[\dot{n}_{CH_4} + x_r\right] \times \left[\dot{n}_{H_2O} - x_r - y_r + z_r\right]}\right) \times \frac{P^2}{n^2_{tot,in} + 2x_r}\right] \quad (19)$$

$$\ln K_S = -\frac{\Delta\bar{g}^0_S}{\bar{R}T_{FC,e}} = \ln\left[\frac{\left(\dot{n}_{CO_2} + y_r\right) \times \left(\dot{n}_{H_2} + 3x_r + y_r - z_r\right)}{\left(\dot{n}_{CO} + x_r - y_r\right) \times \left(\dot{n}_{H_2O} - x_r - y_r + z_r\right)}\right] \quad (20)$$

Furthermore, according to the Faraday's law, the current density can be defined as [21]:

$$j = \frac{n_e F z_r}{N_c A_c} \tag{21}$$

Where A_c and N_c indicate the cell's area and the number of cells in the stack. F denotes the Faraday constant, and n_e refers to the number of electrons that participate in the electrochemical reactions of SOFC which is equal to 2 here [34]. Also, in these equation the temperature unit is considered K.

Moreover, the fuel utilization factor that shows the amount of the consumed fuel (or reacted hydrogen) is calculated as [34]:

$$U_f = \frac{z_r}{\dot{n}_{H_2} + 3x_r + y_r} \tag{22}$$

Furthermore, the generated electrical power by the SOFC stack is given by Ref. [19]:

$$\dot{W}_{SOFC,\ stack,DC} = N_c A_c j V_c \tag{23}$$

$$\dot{W}_{SOFC,stack,\ AC} = \dot{W}_{SOFC,\ stack,\ DC} \times \eta_{inv} \tag{24}$$

The net electrical power generated in the SOFC system is defined by:

$$\dot{W}_{SOFC} = \dot{W}_{SOFC,\ stack,\ AC} - \dot{W}_{FC} - \dot{W}_{AC} \tag{25}$$

The cell voltage is expressed as [34]:

$$V_c = V_N - V_{loss} \tag{26}$$

The Nernst equation is applied to compute the reversible cell voltage as [20]:

$$V_N = -\frac{\Delta G^0}{n_e F} - \frac{\overline{R} T_C}{n_e F} \times \ln\left[\frac{p_{H_2O}}{p_{H_2}\sqrt{p_{O_2}}}\right] \tag{27}$$

Herein, T_C[K] is the stack's operating temperature and p_{H_2}, p_{O_2}, and p_{H_2O} refer to partial pressures. Moreover, the polarization losses can be defined by Ref. [20]:

$$V_{loss} = V_{ohm} + V_{act} + V_{conc} \tag{28}$$

There are other useful relations to calculate the activation, concentration, and Ohmic polarizations that are comprehensively presented in Refs. [35–37].

3.2. Thermoeconomic analysisde

To evaluate the exergoeconomic performance of the energy systems, especially thermodynamic plants, several methods have been proposed, among which the specific exergy costing (SPECO) methodology has been extensively employed to assess the exergoeconomic performance. So, for applying the SPECO method on the energy systems, the cost balance equations and auxiliary equations are used for all elements for obtaining the cost for exergy flows. Following equations is given for cost balance of k^{th} component of the system [38]:

$$\sum \dot{C}_{out,\ k} + \dot{C}_{w,\ k} = \sum \dot{C}_{in,\ k} + \dot{C}_{q,\ k} + \dot{Z}_k \tag{29}$$

Also, Eq. (29) can be rewritten as:

$$\sum (c\dot{E})_{out,k} + c_{w,k}\dot{W}_k = \sum (c\dot{E})_{in,k} + c_{q,k}\dot{E}_{q,k} + \dot{Z}_k \tag{30}$$

Where $\dot{C}$ represents the corresponding cost rate for the inlet and outlet exergy flows, heat and work. Also, $\dot{Z}$ denotes the capital cost which is defined as [38]:

$$\dot{Z}_k = \dot{Z}_k^{CI} + \dot{Z}_k^{OM} \tag{31}$$

In these equations, $\dot{Z}_k^{OM}$ is the operational. and maintenance costs. Also, $\dot{Z}_k^{CI}$ is the annual Levelized capital investing cost of each element, and it's computed by Ref. [38]:

$$\dot{Z}_k^{CI} = \left[\frac{CRF}{\tau}\right] Z_k \tag{32}$$

Where τ indicates the annual operational hours of the cycle and CRF is the capital recovery factor that is defined as follows [39]:

$$CRF = \frac{i_r(1+i_r)^n}{(1+i_r)^n - 1} \tag{33}$$

Where i_r is the interest rate and n is the number of operating years. Moreover, cost of k^{th} component for the year 2018 is considered in the following form [40]:

$$Z_{ref} = Z_0 \times \left[\frac{CEPCI_{ref}}{CEPCI_0}\right] \tag{34}$$

The related cost equations for each component of the proposed system are listed in Table 3.

Furthermore, cost balances as well as the relevant auxiliary relations of each element are provided in Table 4.

For attaining the overall area of the heat exchangers in the proposed system, the total heat transfer coefficient and logarithmic mean temperature difference (LMTD) are considered, hence the total heat transfer area is calculated as follows [41]:

$$A_k = \frac{\dot{Q}_k}{U_k \Delta T_{LMTD}} \tag{35}$$

The overall coefficients of heat transfer for the year 2000 for the heat exchanging components are given in Table 5.

3.3. Evaluation metrics of the suggested system

The first-law efficiency is actually the proportion of the entire generated power to the inlet energy of the cycle. This metric is given by:

$$\eta_I = \frac{\text{Total Product}}{\text{Total Input Energy}} = \frac{\dot{W}_{Net}}{\dot{m}_f \times LHV} \tag{36}$$

$$\dot{W}_{net} = \dot{W}_{SOFC} + \dot{W}_{GT} + \dot{W}_{OFC} - \dot{W}_{AC} - \dot{W}_{FC} \tag{37}$$

The exergy performance and the second law performance are two different concepts. The second law performance is actually the proportion of the real generator work of the cycle to the max plausible work that is happened in the reversible procedure. While the exergy performance is defined as the proportion of the useful or generated exergy to the input exergy and is presented by:

$$\eta_{II} = \frac{\text{Total Generated Exergy}}{\text{Total Input Exergy}} = \frac{\dot{W}_{Net}}{\dot{E}x_5 + \dot{E}x_{16}} \tag{38}$$

Also, the sum unit cost of the product for the devised system is calculated as:

Table 3
Cost function equations for components of proposed system.

Components	Cost functions	Ref. year	Cost index
Gasifier	$Z_G = 1600 \times (\dot{m}_{drybiomass})^{0.67}$	2014	576.1
Air preheater	$Z_{AP} = 130 \times \left(\frac{A_{AP}}{130}\right)^{0.78}$	2005	468
Air compressor	$Z_{AC} = 91562 \left(\frac{\dot{W}_{AC}}{455}\right)^{0.67}$	2003	402
Air heat exchanger	$Z_{AHX} = 130 \times \left(\frac{A_{AP}}{130}\right)^{0.78}$	2005	468
Fuel compressor	$Z_{FC} = 91562 \left(\frac{\dot{W}_{AC}}{455}\right)^{0.67}$	2003	402
Mixer	$Z_{Mixer} = 0$	–	–
SOFC stack	$Z_{SOFC} = A_{act} N_{cell} (2.9 T_{cell} - 1907)$	2007	525
Inverter	$Z_{inv} = 10^5 \left(\frac{\dot{W}_{stack}}{500}\right)^{0.7}$	2002	396
Afterburner	$Z_{CC} = \left(\frac{46.08 \times \dot{m}_{10}}{0.995 - P_{out}/P_{in}}\right) \left[1 + \exp(0.018 T_{AB}) - 26.4\right]$	1994	368
Gas turbine	$Z_{GT} = \left(\frac{479.34 \times \dot{m}_{12}}{0.92 - \eta_{GT}}\right) \ln\left(\frac{P_{13}}{P_{12}}\right) \times [1 + \exp(0.036 T_{12}) - 54.4]$	1994	368
Heat exchanger	$Z_{H.X.} = 309.14(A_{H.X.})^{0.85}$	2001	394.1
Turbine	$Z_{Tur,OFC} = 4750 \times \dot{W}_{tur}{}^{0.5}$	2001	394.1
Mixer	$Z_{Mixer} = 0$	–	–
Flash evaporator	$Z_{flash} = 0$	–	–
Pump	$Z_{pu} = 200(\dot{W}_{pu})^{0.65}$	2001	394.1
Throttling valve	$Z_{E.V} = 114.5 \times \dot{m}_{22}$	2001	394.1
Condenser	$Z_{cond} = 516.62 \times (A_{cond})^{0.6}$	2001	394.1

Table 4
Cost rate balances and auxiliary equations for components of proposed system.

Component	Cost balance	Auxiliary equations
Gasifier	$\dot{Z}_{G,PY} + \dot{C}_5 + \dot{C}_{16} = \dot{C}_6$	$c_5 = 2$ \$/GJ , $c_{16} = 0$
Fuel blower	$\dot{Z}_{FC,PY} + \dot{C}_6 + \dot{C}_{W,FC} = \dot{C}_7$	$c_{W,FC} = c_{W,SOFC,AC}$
Air Heat exchanger	$\dot{Z}_{AHX,PY} + \dot{C}_{11} + \dot{C}_2 = (\dot{C}_{3a} + \dot{C}_{12})$	$c_{11} = c_{12}$
Anode mixer	$\dot{Z}_{AM,PY} + \dot{C}_7 + \dot{C}_{8b} = \dot{C}_8$	N/A
Cathode mixer	$\dot{Z}_{CM,PY}(0) + \dot{C}_{3b} + \dot{C}_{3a} = \dot{C}_3$	N/A
SOFC Stack	$\dot{Z}_{SOFC,stack,PY} + (\dot{C}_3 + \dot{C}_8) = (\dot{C}_4 + \dot{C}_9) + \dot{C}_{W,SOFC,stack}$	$c_9 = c_{W,SOFC,DC}$, $c_4 = c_{W,SOFC,DC}$
Afterburner	$Z_{AB,PY} + \dot{C}_{4a} + \dot{C}_{9b} = \dot{C}_{10}$	$c_{9b} = c_{8b}$, $c_{4a} = c_{3b}$ $c_{9b} = c_9$, $c_{4a} = c_4$
Inverter	$\dot{Z}_{INV,PY} + \dot{C}_{W,SOFC,DC} = \dot{C}_{W,SOFC,AC}$	N/A
Air preheater	$\dot{Z}_{Ap,PY} + \dot{C}_{10} + \dot{C}_{15} = \dot{C}_{11} + \dot{C}_{16}$	$c_{16} = c_{15}$, $c_{10} = c_{11}$
Gas turbine	$\dot{Z}_{GT,PY} + \dot{C}_{12} = (\dot{C}_{13} + \dot{C}_{w,GT})$	$c_{13} = c_{12}$
Compressor	$\dot{Z}_{AC,PY} + \dot{C}_1 = (\dot{C}_2 + \dot{C}_{W,AC})$	$c_1 = 0$, $c_{W,AC} = c_{W,SOFC,AC}$
Heat exchanger	$\dot{Z}_{HX,PY} + \dot{C}_{13} + \dot{C}_{17} = (\dot{C}_{14} + \dot{C}_{18})$	$c_{17} = c_{18}$
Flash evaporator	$\dot{Z}_{Eva,PY} + \dot{C}_{18} = (\dot{C}_{20} + \dot{C}_{22})$	$c_{20} = c_{22}$
Turbine	$\dot{Z}_{T,PY} + \dot{C}_{20} = (\dot{C}_{21} + \dot{C}_{W,T})$	$c_{20} = c_{21}$
Mixer	$\dot{Z}_{M,PY}(0) + \dot{C}_{21} + \dot{C}_{23} = \dot{C}_{24}$	N/A
Throttling valve	$\dot{Z}_{th.v,PY} + \dot{C}_{22} = \dot{C}_{23}$	$c_{22} = c_{23}$
Condenser	$\dot{Z}_{Cond,PY} + \dot{C}_{24} + \dot{C}_{26} = (\dot{C}_{25} + \dot{C}_{27})$	$c_{24} = c_{25}$
Pump	$\dot{Z}_{pm,PY} + \dot{C}_{W,pm} + \dot{C}_{25} = \dot{C}_{17}$	N/A

Table 5
Heat transfer coefficients for heat exchangers of the proposed system.

Components	U [W/m^2·K]
Air preheater	1000
Air heat exchanger	1000
Heat exchanger	900
Condenser	1100

$$c_{p,tot} = \frac{\sum_{i=1}^{n_k} \dot{Z}_k + \sum_{i=1}^{n_F} \dot{C}_{F_i}}{\sum_{i=1}^{k} \dot{E}_{p_i}} \tag{39}$$

Throughout the system's lifetime, the total investment gain is presented as the net present value (NPV), which is expressed as [1]:

$$NPV = -C_0 + CF\frac{(1+r)^N - 1}{r(1+r)^N} \tag{40}$$

Where N denotes the project's lifetime, which is considered 20 years in this study, CF is the annual income cash flow, C_0 is the investment cost of total system, and r represents the discount factor, which is considered 3%.

A new criterion is defined for evaluating the system performance from the environmental viewpoint in the present work. Levelized total emissions (LTE) expresses the ratio of the pollutants and greenhouse gasses emissions during the considered lifetime to the net produced power.

$$LTE = \frac{\text{Total Emissions During The Cycle Lifetime}}{\text{Net Generated Power}} = \frac{\dot{m}_{CO_2,\ emmited}}{\dot{W}_{Net}} \tag{41}$$

3.4. Multi-objective optimization

A common problem in designing energy systems is facing various conflicting objectives. Optimizing the energy system can resolve this issue and help engineers devise high-efficient and economical energy systems. Typically, the conflicting objectives may be exergy efficiency, power generation, total product cost, total cost rate, Levelized emissions, and hydrogen production rate. Selecting the conflicting objectives correlates with the perspective of the decision-makers. The system operates at a wide range of operating points. Accordingly, the system should be optimized for efficient and affordable operation; so the system can be designed based on the optimum operating conditions. For the optimization process in the present study, a robust computational code is developed in Matlab software. In the present work, the proposed multi-objective problem (MOP) is solved by the multi-objective particle swarm optimization (MOPSO) approach in Matlab to find the most preferred solutions. Finally, the Technique for Order Performance by Similarity to Ideal Solution (TOPSIS) method is applied to select the final optimal solution [31].

The decision parameters varied in particular intervals to attain the best solution points, and along with the decision parameters, the other parameters of the system are calculated. Six primary decision parameters are assumed to achieve the optimal values under the proposed multi-objective optimization approach. In this paper, three factors are considered as objectives, including total product cost, Levelized total emission, and exergy efficiency as:

$$Min\{-\eta_{II}, LTE\ ,\ c_{p,tot}\} \tag{42}$$

The range of decision variables for the parametric analysis is given in Table 6.

Table 6
Domain of major decision parameters.

Parameter	Range
Current density (j)	$3000 < j < 4000$ [A/m^2]
Stack temperature difference (ΔT_{stack})	$95 < \Delta T_{stack} < 120$ [°C]
Utilization factor (U_f)	$0.60 < U_f < 0.86$[–]
Anode recyling ratio (R_{AR})	$0.10 < R_{AR} < 0.42$ [–]
Air blower pressure ratio (PR_{AC})	$1.25 < PR_{AC} < 2.50$ [–]
Fuel blower pressure ratio (PR_{FC})	$1.25 < PR_{FC} < 2.50$ [–]

4. Result and discussion

In this section, the effort has been made to present the modeling results via EES for the proposed power generation system. Firstly, for verifying the validity of the modeling procedure, the results are compared with the available data in the literature. Then, to deliver the parametric study, the base system with basic operating parameters is defined, and subsequently, the effect of various parameters on the system performance is determined. Afterward, the results of the optimization procedure are comprehensively presented.

4.1. Model validation

Any energy system's validity will be proven when the outputs related to each of its sub-systems be validated. Accordingly, in the present study, results reported by Tao et al. [42] are considered to validate the SOFC component. On the other hand, to ensure the obtained data for the biomass gasification unit, the results of three reliable reference works, including Gholamian et al. [43], Zainal et al. [44], and Alauddin [45], are considered. In the validation procedure, all of the problem conditions and assumptions are considered similar between the current investigation and reference investigations.

The results of the validation are presented in Fig. 3a and b for SOFC and gasifier units, respectively. As Fig. 3a demonstrates, the results of the present modeling fit well on available experimental results with a maximum relative error of 4.77%. Also, as indicated in Fig. 3b for the gasification process and considering the root mean squared deviation (RMSD) metric, the results obtained here are in excellent agreement with those of experimental and other numerical works. The reason for the deviation could be found in the method of problem modeling and the difference of softwares in which the computational codes have been developed.

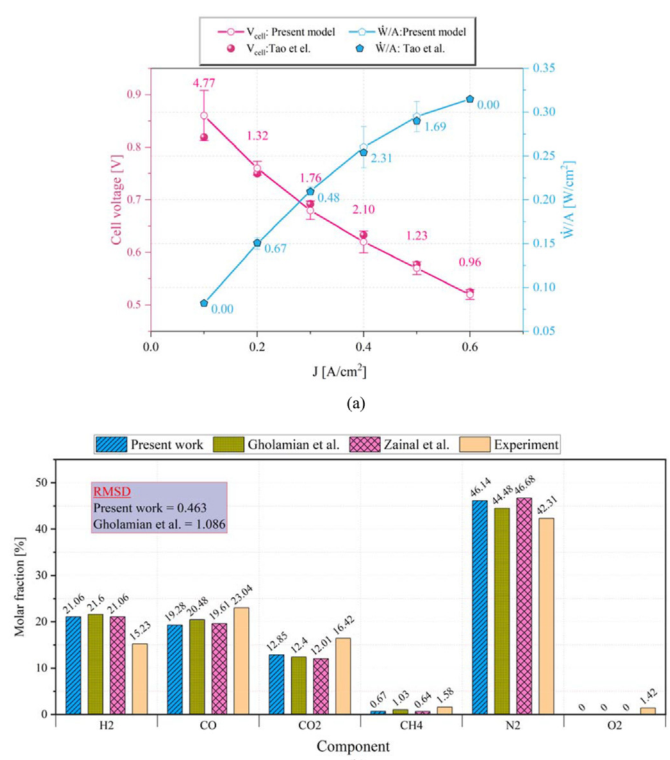

Fig. 3. Validation of modeling results for the a) SOFC stack and b) Gasification unit.

4.2. Results of the modeling for the base system

In this sub-section, the effort has been made to present the results of the base system with input parameters as listed in Table 1. Thermodynamic modeling is started by calculating all the required thermophysical characteristics of the state points in the system. The outputs of the thermophysical characteristics are presented in Table 7.

The main performance criteria for the suggested power generation system are presented in Table 8, where the net output power is obtained 425.39 kW.

The power generation and utilization of the power-based components of the system are presented in Fig. 4. As shown, due to the high flow rate of air, the air compressor is contributed to the highest power utilization rate by 34.45 kW. The electrical power consumption rate of the fuel blower, pump, and compressor is atoned by the power generated within the turbine in the OFC subsystem, which bolsters the idea of the combination of the SOFC/GT with OFC. More from Table 8, the energetic and exergetic efficiencies of the proposed plant is calculated by 49.37% and 42.50%, respectively. Also, the total cost of products and Levelized total emission for are obtained as 5.52 $/GJ and 29.62 t/MWh.

The exergy flow, as well as the exergy destruction rate of each component in the devised system is shown in Fig. 5. According to the second-law principle of the thermodynamic, the term irreversibility is defined as the destruction of the exergy. The main reasons for the irreversibility of any process are the heat transfer and pressure drop within the components of the plant. Based on Fig. 5, the maximum rate of exergy destruction belongs to air heat exchanger. From 1001 kW input exergy, 229.60 kW is destructed in the air heat exchanger. Also, it can be seen that the OFC subsystem holds a lower exergy destruction rate, where, from the total input exergy, only 41.55 kW is destroyed in the OFC cycle. The rate of exergy loss is also considered in the Grossman diagram, which is calculated by 2.48 kW. The total useful exergy is obtained by 425.39 kW; thus, the exergetic efficiency calculated as 42.50%.

Table 8
Main simulation outputs of proposed system at base conditions.

Performance index	Value	Unit
Net output power ($\dot{W}_{net}$)	425.39	[kW]
Energy efficiency (η_{I})	49.37	[%]
Exergy efficiency (η_{II})	42.45	[%]
Levelized total emission of the system (LTE)	29.62	[t/MWh]
Total exergy destruction ($\dot{E}_{D,\ tot}$)	575.61	[kW]
Total product cost ($c_{P,\ tot}$)	5.52	[$/GJ]

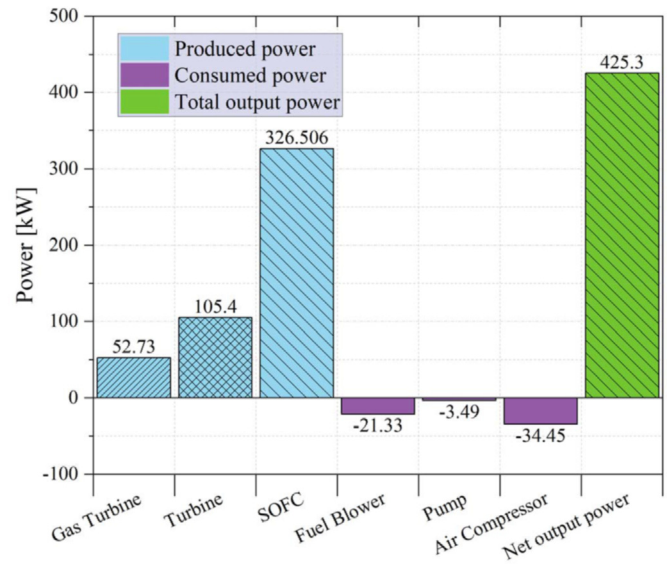

Fig. 4. Generated and consumed electricity in the proposed system.

Table 7
Characteristics at state points of the system.

State	T[°C]	P[kPa]	$\dot{E}x$ [kW]	$\dot{m}$ [kg/s]	c [$/GJ]	$\dot{C}$[$/h]
1	25.00	101.32	7.30	1.67	0.00	0.00
2	45.82	122.60	35.27	1.67	5.53	0.70
3a	661.10	120.20	516.70	1.67	7.18	13.35
3	726.85	117.80	1050	2.70	5.08	22.18
3b	826.85	115.40	534.60	1.03	4.59	8.83
4	826.85	115.40	1249	2.65	4.59	20.63
4a	826.85	115.40	749.50	1.59	4.59	12.38
5	25.00	101.32	1001	0.05	2.00	7.21
6	610	101.30	862.70	0.09	2.44	7.59
7	640.10	122.60	850.30	0.09	2.56	7.99
8	726.85	122.60	1042	0.18	2.91	10.90
8b	826.85	120.10	178	0.09	2.94	4.59
9	826.85	120.10	445	0.23	4.59	7.35
9b	826.85	120.10	267	0.14	4.59	4.41
10	902.10	109.70	954.60	1.73	4.90	16.80
11	893.70	107.50	938.40	1.73	4.90	16.60
12	356.10	105.30	227.40	1.73	4.90	4.01
13	328.10	84.05	171.90	1.73	4.90	3.03
14	43.39	85.30	2.48	1.73	4.90	14.50
15	25	101.30	0.00	0.04	0.00	0.00
16	500	101.30	7.16	0.04	1.84	0.30
17	35.95	2735	3.395	0.92	5.00	0.06
18	285.90	2735	152.4	0.92	3.92	2.14
19	230	1231	147.5	0.93	3.05	1.62
20	230	1231	108.6	0.55	0.25	0.097
21	90	2.21	4.932	0.55	0.25	0.004
22	230	1231	38.89	0.38	0.53	0.074
23	37.48	2.21	0.24	0.38	2.52	0.002
24	69.56	2.21	4.32	0.92	0.32	0.004
25	35	6.25	0.81	0.92	0.32	0.001
26	15	100	0.00	9.97	0.00	0.00
27	25	100	0.025	9.97	3.99	0.82

Moreover, the contribution of each component in the total exergy destruction rate is plotted in Fig. 6. As can be seen from Fig. 6 that the air heat exchanger is responsible for 40% of total exergy destruction as the highest value. Also, the OFC subsystem holds 7.25% of the total exergy destruction rate. Among different components of the OFC unit, the turbine holds the maximum irreversibility by 2.67%, which is followed by the condenser with 1.94% of the total exergy destruction rate. The lowest irreversibility rate is associated with the OFC heat exchanger, with 0.16% of the total exergy destruction rate.

Table 9 presents the results of the exergy and exergoeconomic analysis for each component of the proposed system. The highest investment cost ($\dot{Z}$) amongst various components in the system refers to SOFC stack by 0.54 $/h. Another parameter of Table 9 is the cost of exergy destruction, in which the greatest rate of exergy destruction cost lies in the gas turbine by 4.05 $/h. This is due to the fact that the turbine has a relatively great exergy destruction rate and fuel cost.

4.3. Parametric analysis

Parametric analysis is performed to study the effect of the leading effective parameters on performance, economic, and emissions indicators and compare the results. The range of decision variables for the parametric analysis is given in Table 6. The main findings of the parametric study are presented in Figs. 7–12.

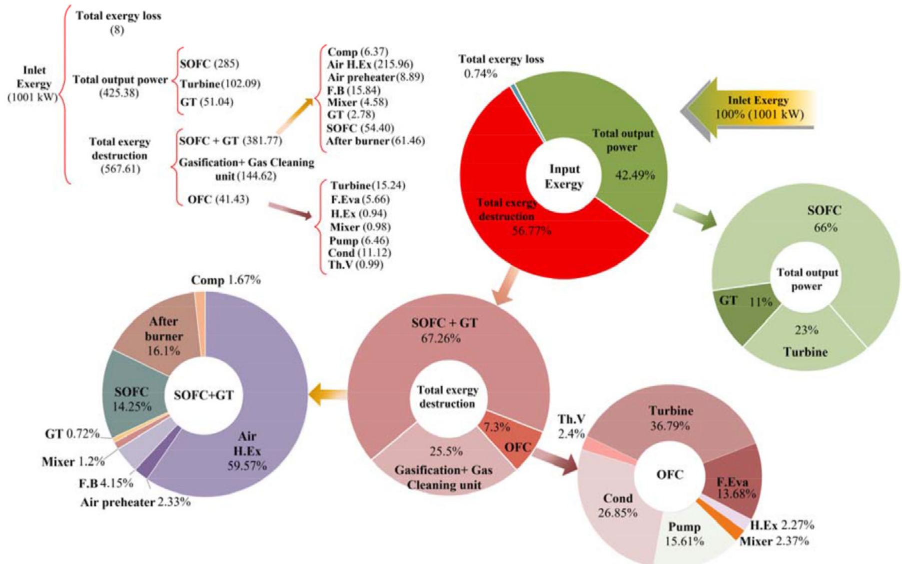

Fig. 5. Exergy flow and share of exergy destruction from total input exergy for each component of the system.

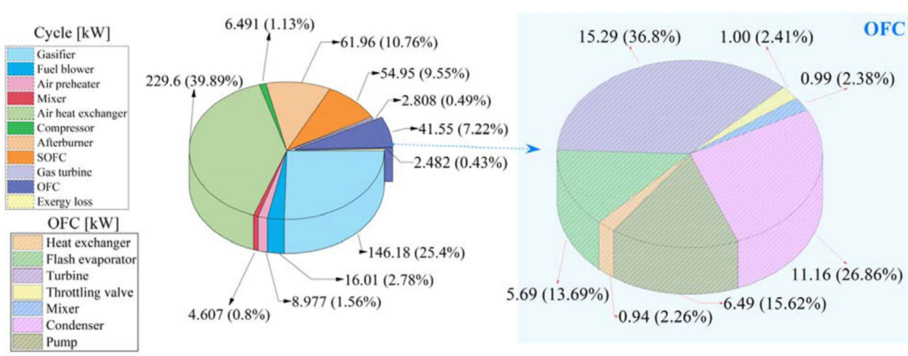

Fig. 6. Contribution of each component of the system to total exergy destruction.

Table 9
Results of exergy and exergoeconomic analyses.

Component	$\dot{E}_F$ [kW]	$\dot{E}_P$ [kW]	$\dot{E}_D$ [kW]	η_{II} [%]	c_F [\$/GJ]	c_P [\$/GJ]	$\dot{C}_L$ [\$/h]	$\dot{C}_D$ [\$/h]	$\dot{Z}$ [\$/h]
Gasifier	1008	862.70	146.18	85.57	2.07	2.44	0	1.09	0.07
Fuel blower	21.33	5.32	16.01	24.92	4.98	1.78	0	0.29	0.026
Air Compressor	34.45	27.96	6.49	81.16	4.98	5.77	0	0.12	0.03
Air heat exchenger	711.00	481.40	229.60	67.71	4.90	7.30	4.05	4.05	0.10
Gas turbine	55.53	52.73	2.81	94.94	4.90	4.39	0.05	0.05	0.04
Cathode mixer	1051	1040	11.02	99.90	5.86	4.74	0	0.02	0
Anode mixer	1046	1042	3.99	99.66	2.90	2.91	0	0.03	0
Inverter	321.50	310.40	11.10	95.00	4.59	4.09	0	0.28	0.17
SOFC stack	2093	2038	54.95	97.37	4.40	4.59	0	0.87	0.54
After burner	1017	954.60	61.96	93.90	4.59	4.90	0	1.02	0.06
Heat exchenger	16.13	7.16	8.98	44.36	4.90	11.84	0.15	0.16	0.02
Pump	9.49	2.99	6.45	85.93	6.84	6.64	0	0.16	0.0006
Flash Evaporator	174.30	173.40	0.94	99.90	4.90	4.94	0	0.02	0.0080
Turbine	120.70	105.40	15.29	87.33	5.44	6.84	0	0.30	0.23
Condenser	7.08	4.08	2.99	57.73	31.79	35.41	0	0.34	0.0050
Mixer	11.20	4.33	6.87	99.90	5.82	6.35	0	0.23	0.02
System	7697.74	7112.47	585.66	42.50	34.45	128.58	4.25	8.80	1.31

4.3.1. Effect of the SOFC stack's temperature difference on the main performance criteria

Fig. 7 presents the effect of temperature difference of the SOFC stack (ΔT_{stack}) on the main performance criteria. As shown, by the increment of ΔT_{stack} from 95 to 120°C, net output power, and consequently, the energy and exergy efficiencies increase. The main reason for these trends is that with consideration of a constant temperature value at the SOFC inlet, by augmentation of ΔT_{stack}, the

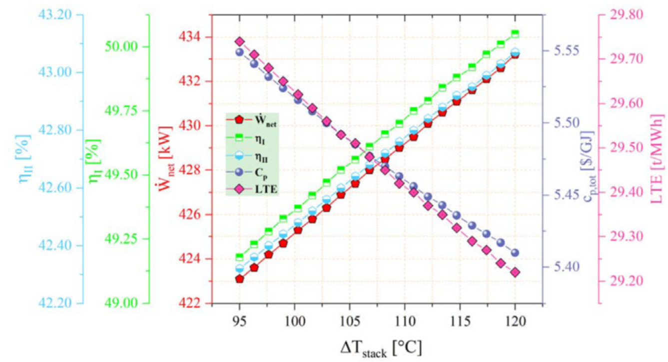

Fig. 7. Effect of the SOFC stack's temperature difference on the main performance criteria.

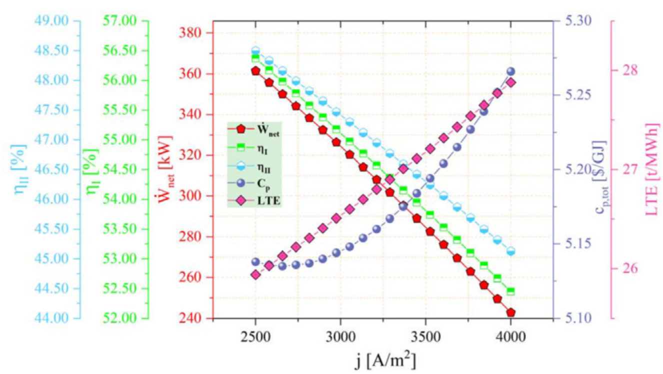

Fig. 8. Effect of the current density on the main performance criteria.

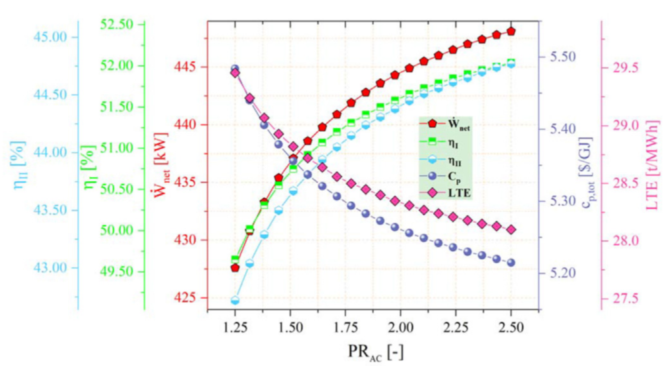

Fig. 9. Effect of the air compressor pressure ratio mass on the main performance criteria.

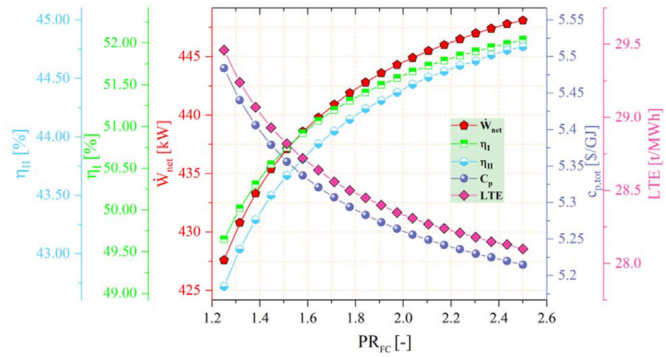

Fig. 10. Effect of the fuel blower pressure ratio on the main performance criteria.

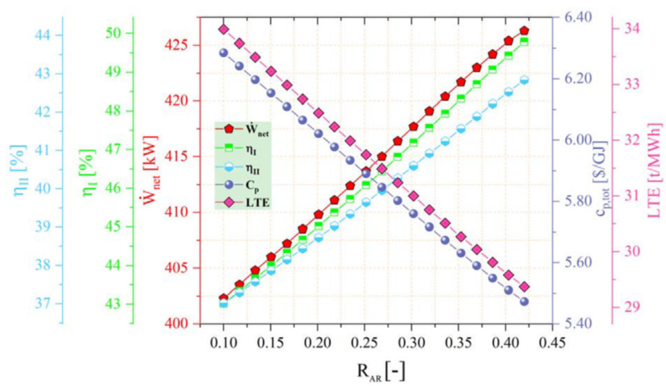

Fig. 11. Effect of the anode recycling ratio on the main performance criteria.

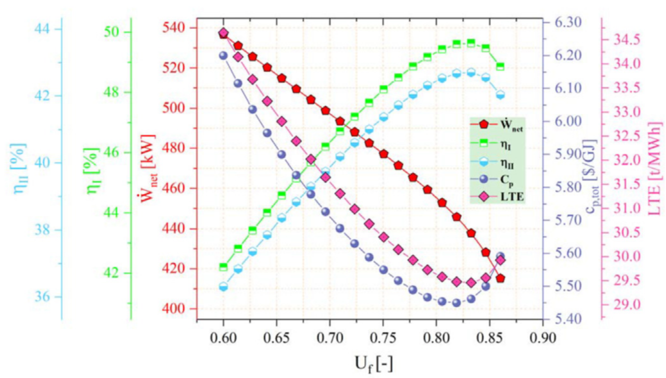

Fig. 12. Effect of the fuel utilization factor on the main performance criteria.

outlet temperature of the SOFC stack increases; hence, the inlet temperature of the gas turbine and OFC heat exchanger increases; as a result, the power generated by the gas turbine and OFC turbine increases. Thus, the net output power, energy efficiency, and exergy efficiency increase subsequently. With the increment of net output power, the total cost of product and Levelized total emission values decrease.

4.3.2. Effect of the current density on the main performance criteria

Fig. 8 represents the effect of the current density on the net output power, energy efficiency, exergy efficiency, total cost of products, and Levelized total emission. As Fig. 8 demonstrates, by the increment of current density, the SOFC power output decreases due to the increment of overpotentials. As a result, the net output power decreases, which is proportional to the changes in the output power of the SOFC stack, which has a direct effect on the power capacity according to the net power equation. Similarly, according to total energy efficiency and exergy relations, the energy and exergy efficiency of the whole system decrease. With the decrement of net output power, the total cost of product and Levelized total emission values increase.

4.3.3. Effect of the air compressor pressure ratio mass on the main performance criteria

Fig. 9 illustrates the effect of the air compressor pressure ratio on the main performance indicators. This figure indicates that by incrementing the air compressor pressure ratio from 1.25 to 2.50,

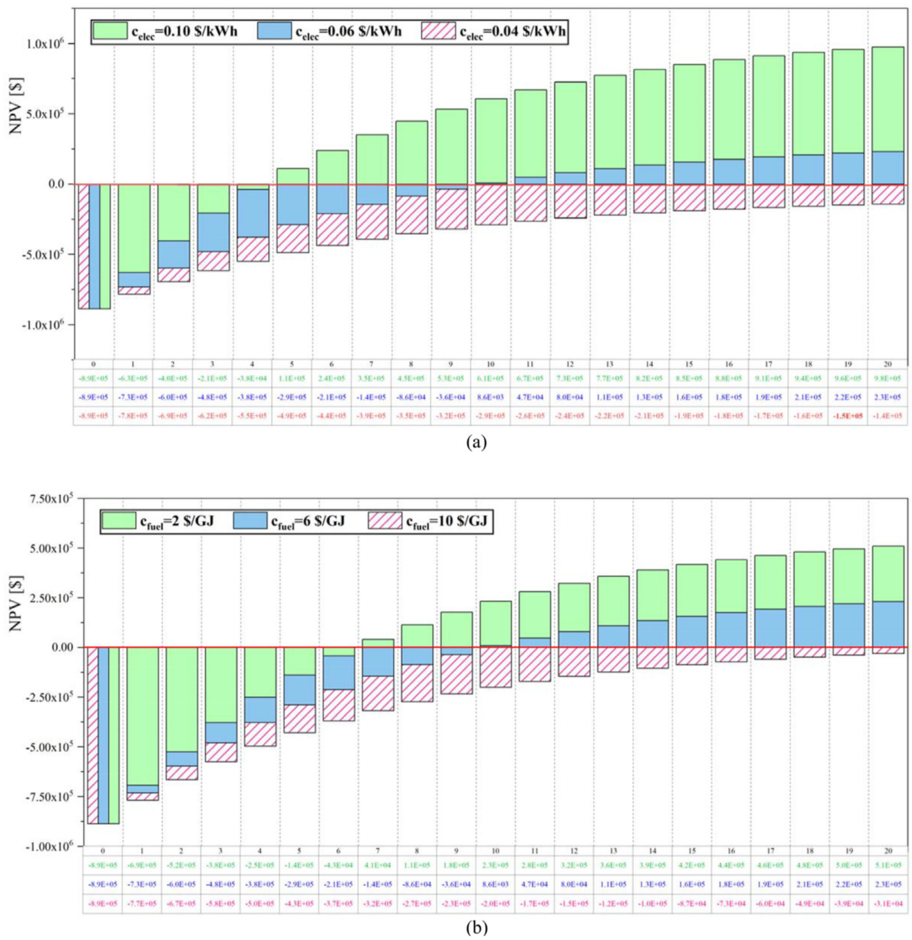

Fig. 13. Effect of a) electricity price and b) fuel cost on net present value in all of the years during system's lifetime.

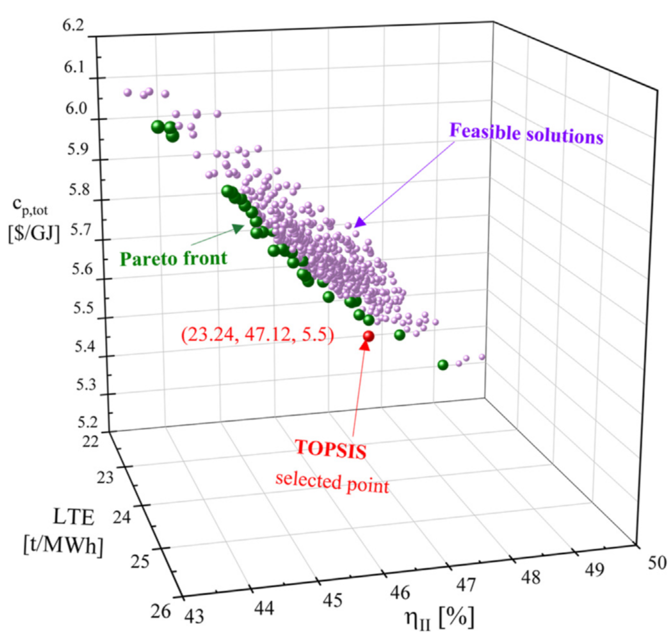

Fig. 14. The Pareto frontiers of the proposed models as optimal solutions for total product cost, exergy efficiency, and Levelized total emission as objective functions.

net output power, energy efficiency, and exergy efficiency increase while the total cost of products and Levelized total emission decrease significantly. The main reason for this variation is that as the PR_{AC} increases, the power generation capacity of the SOFC and gas turbine increases; therefore, the electrical power increases. Considering the total cost and LTE relations with the total power of the system, total cost and LTE decrease.

4.3.4. *Effect of the fuel blower pressure ratio on the main performance criteria*

Fig. 10 shows the effects of fuel blower pressure ratio on net output power, energy and exergy efficiencies, the total cost of products, and Levelized total emission. By incrementing the fuel blower pressure ratio, the output power of the gas turbine increases; thus, the net output power increases. By increasing the total output power, energy and exergy efficiencies increase. Moreover, by the increment of net output power, the unit cost of the product decreases, and then the total cost of the product decreases. Finally, the Levelized total emission decreases with the increment of the fuel blower pressure ratio.

4.3.5. *Effect of the anode recycling ratio on the main performance criteria*

As a key parameter in the system analysis, the anode recycling ratio (R_{AR}) can affect the system's performance indices, including net output power, energy efficiency, exergy efficiency, the total cost of products, and Levelized total emission, as illustrated in Fig. 11.

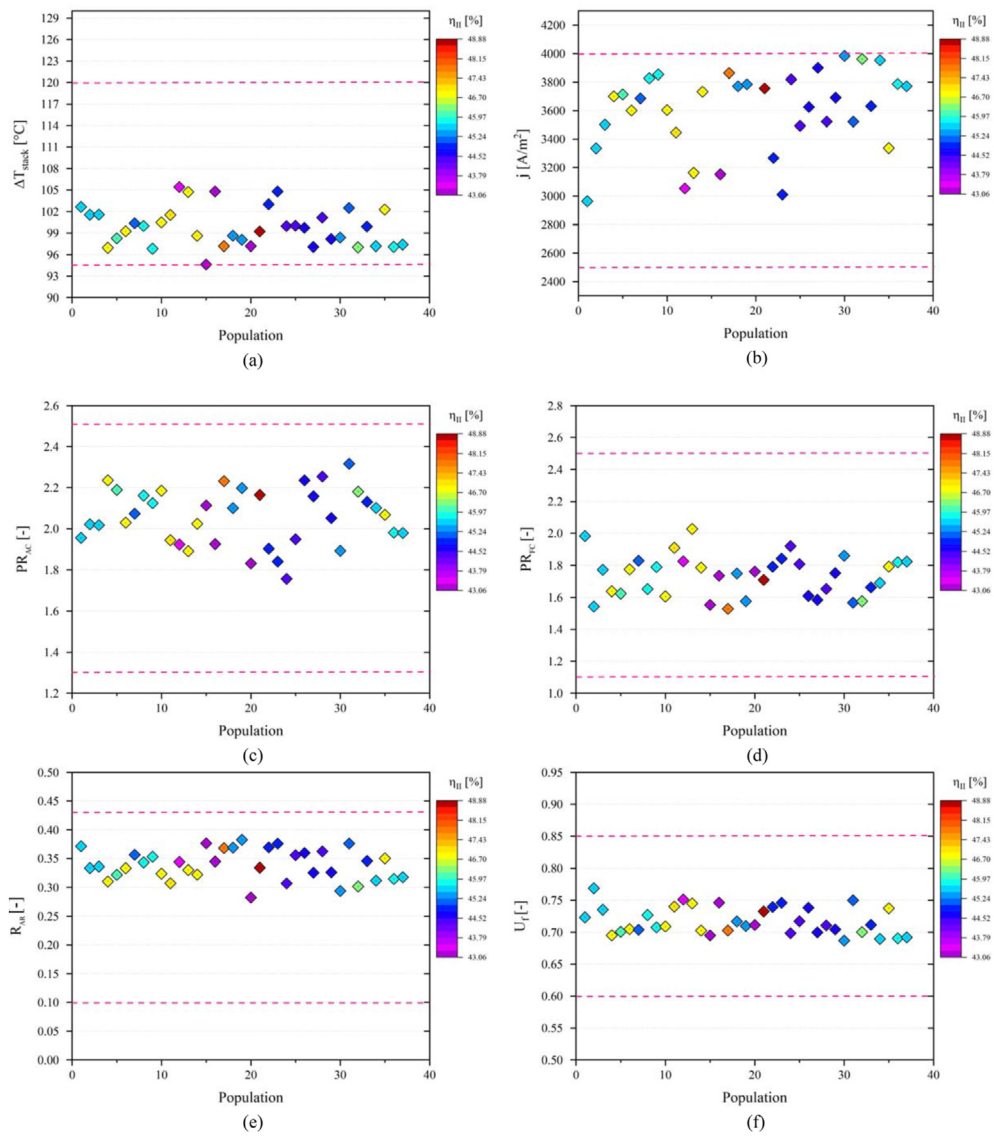

Fig. 15. Scatter distribution of the effective parameters.

The figure indicates that by incrementing of the anode recycling ratio (R_{AR}), the output power of the SOFC increases, and the power consumption of fuel blower decreases; thus, the net output power of the system increases considerably. By increment of the total output power, energetic and exergetic efficiencies increase subsequently. Furthermore, the figure indicates that augmentation of R_{AR} would decrease the total product costs and Levelized total emission.

4.3.6. Effect of the fuel utilization factor on the main performance criteria

Fig. 12 shows the effects of the fuel utilization factor (U_f) on the main performance indicators. According to Fig. 12, as the U_f increases from 0.60 to 0.86, the power generation capacity of the system initially increases and then decreases. Following the power trend and concerning the power the energy and exergy efficiencies, these values reach a maximum value and drops then. Due to the power generation variation trend, the corresponding cost and since the exergy of generated power increased and after that decreased, so according to the total cost relation, the total cost of products of the entire system is reduced and then increased. Moreover, from Fig. 12, the LTE value is decreased to a minimum value and increased after that.

4.4. Net present value and payback period

In this sub-section, a sensitivity analysis is performed for investigating two economic methods, including payback period and net present value.

Fig. 13a and b illustrate the effect of electricity selling price (c_{elec}) and fuel purchasing cost (c_{fuel}) on the NPV in plant lifetime, respectively. Fig. 13a illustrates the NPV variation for $c_{fuel} = 6$ \$/GJ and different electricity selling value. Based on this figure, it can be seen for electricity selling price of 0.04 \$/kWhand lower, the total value of NPV at the end of plant is negative, so, the construction of such plant is not feasible from the economic viewpoint. However, considering $c_{fuel} = 6$ \$/GJ for purchasing the fuel and $c_{elec} = 0.06 - 0.10$ \$/kWh for selling the electricity, it would be stated that the construction of such plant is available from the economic perspective in most countries. For instance, for $c_{fuel} = 6$ \$/GJ and

c_{elec} = 0.10 \$/kWh, the total NPV value for the plant lifetime is 9.8 × 10^5 \$. Also, based on this figure, the payback period (PP) drops from 9.75 years for c_{elec} = 0.06 \$/kWh to 4.25 years for c_{elec} = 0.10 \$/kWh.

Also, the effect of fuel purchase price at c_{elec} = 0.06 \$/kWh is shown in Fig. 13b. For fuel price higher than 10 \$/GJ , the value of the total NPV is negative at the end of plant lifetime. So, for this plant it takes more than 20years to be profitable, hence, it is not feasible economically to set up such plant. However, for fuel cost of 6 \$/GJ and lower, the plant can be profitable after some years of working. Moreover, the payback period increases from 6.5 years to 9.8 years as the fuel cost increases from c_{fuel} = 2 \$/GJ to c_{fuel} = 6 \$/GJ.

4.5. Optimization results

The Pareto frontier obtained by MOPSO is demonstrated in Fig. 14. As can be seen, none of Pareto's results dominates the other. Each of the points in the Pareto frontier could be considered as an optimal solution. Hence, a decision-making method should be used for selecting the appropriate point based on the design requirements. The final optimal solution selected by the TOPSIS decision-making method is η_{II} = 47.12%, LTE = 23.24 t/ MWh, and $c_{p,tot}$ = 5.50 \$/GJ.

The scatter distribution of six decision variables for the proposed power generation system is presented in Fig. 15. As pictured in this figure, scatter distribution gives a suitable visual overview of the results obtained by MOPSO, related to the design parameter of the last population in the feasible set. 15a presents the distribution of ΔT_{stack}, almost all of the optimum solutions are concentrated around the lower boundary, which means that at this temperature (close to 94°C) the proposed system has the optimum efficiency. Fig. 15b shows the distribution of current density on the whole interval between $2500 < j < 4000$, in which most of the solution points are focused below 4000. According to Fig. 15c, it is observed that the optimal points of PR_{AC} are located between 1.75 and 2.3. The distribution of the optimal points for the PR_{FC} is presented in Fig. 15d. As is observed, the optimum points are located at the ranges of 1.5 and 2. Fig. 15e shows R_{AR} distribution; most of the optimum solution points are located between 0.30 and 0.40. Fuel utilization factor distribution is shown in Fig. 15f, the most of the optimum points values are between 0.68 and 0.75, which means the optimum power generation can be obtained in this range.

5. Conclusion

In the present paper, a combined biomass-based solid oxide fuel cell/gas turbine/organic flash cycle is proposed considering air as the gasification agent. The thermal energy of the solid oxide fuel cell's exhaust gases is recovered in a gas turbine and organic flash cycle to enhance the power generation. The devised power generation system is then thoroughly studied from the energy, exergy, economic, and environmental viewpoints. Ultimately, the proposed system is optimized by a multi-objective optimization method considering exergy efficiency, total product cost, and Levelized total emissions as objective functions. The main conclusions of this study may be summarized as:

- For the base simulation inputs, the energy and exergy efficiencies of the proposed system is obtained by 49.37% and 42.50%, respectively. Also, net output power, Levelized total emission, and total product cost are computed by425.39 kW, 29.62 t/MWh, and 5.52 \$/GJ, respectively.
- By increasing the temperature difference of the fuel cell, the net output power increases; as a result, the energy and exergy efficiencies increase to the highest point.
- For the fuel cost of 6 \$/GJ and electricity price of 0.10 \$/kWh, the total net present value at the end of plant lifetime is 9.8 × 10^5 \$ and the payback period is 4.25 years.
- The optimal solution selected by the TOPSIS method is obtained by η_{II} = 47.12%, LTE = 23.24 t/MWh, and $c_{p,tot}$ = 5.50 \$/GJ.

Author statement

All authors who meet authorship criteria are listed as authors, and all authors certify that they have participated sufficiently in work to take public responsibility for the content, including participation in the concept, design, analysis, writing, or revision of the manuscript. Furthermore, each author certifies that this material or similar material has not been and will not be submitted to or published in any other publication. The authors' contributions to this work are described as follows:

Cai Cheng conceived the research idea, conducted the initial analysis, collected data, and authored the majority of the text. ***Hosein Niroumandi*** authored parts of the text, reviewed the analysis, proposed changes, and contributed to data collection. ***Jacob Cherian*** developed the parametric analysis models and the code for the figures and checked and contributed to the analysis. ***Umer Zaman*** reviewed and edited the manuscript and contributed parts of the text. ***Muhammad Safdar Sial*** conceptualized the study, developed the methodology for the screening of the data set, proposed the conceptual design of the model, and provided significant input into the research coordination, collected data, edited the manuscript and contributed parts of the text.

All authors made significant contributions and revisions to the manuscript itself.

Declaration of competing interest

The authors declare that they have no known competing financial interests or personal relationships that could have appeared to influence the work reported in this paper.

References

[1] Hamrang F, Shokri A, Mahmoudi SM, Ehghaghi B, Rosen MA. Performance analysis of a new electricity and freshwater production system based on an integrated gasification combined cycle and multi-effect desalination. Sustainability 2020;12:7996.
[2] Hosseinpour J, Chitsaz A, Liu L, Gao Y. Simulation of eco-friendly and affordable energy production via solid oxide fuel cell integrated with biomass gasification plant using various gasification agents. Renew Energy 2020;145:757–71.
[3] Menikpura SNM, Sang-Arun J, Bengtsson M. Integrated solid waste management: an approach for enhancing climate co-benefits through resource recovery. J Clean Prod 2013;58:34–42.
[4] Liu W, Cui Y, Du X, Zhang Z, Chao Z, Deng Y. High efficiency hydrogen evolution from native biomass electrolysis. Energy Environ Sci 2016;9:467–72.
[5] Gassner M, Vogel F, Heyen G, Maréchal F. Optimal process design for the polygeneration of SNG, power and heat by hydrothermal gasification of waste biomass: thermo-economic process modelling and integration. Energy Environ Sci 2011;4:1726–41.
[6] Shayan E, Zare V, Mirzaee I. Hydrogen production from biomass gasification; a theoretical comparison of using different gasification agents. Energy Convers Manag 2018;159:30–41.
[7] Sharma S, Sheth PN. Air–steam biomass gasification: experiments, modeling and simulation. Energy Convers Manag 2016;110:307–18.
[8] Balu E, Lee U, Chung JN. High temperature steam gasification of woody biomass–a combined experimental and mathematical modeling approach. Int J Hydrogen Energy 2015;40:14104–15.
[9] Schuster G, Löffler G, Weigl K, Hofbauer H. Biomass steam gasification–an extensive parametric modeling study. Bioresour Technol 2001;77:71–9.
[10] Bartela Ł, Kotowicz J, Remiorz L, Skorek-Osikowska A, Dubiel K. Assessment of

the economic appropriateness of the use of Stirling engine as additional part of a cogeneration system based on biomass gasification. Renew Energy 2017;112:425–43.
[11] Dimitrova Z, Maréchal F. Environomic design for electric vehicles with an integrated solid oxide fuel cell (SOFC) unit as a range extender. Renew Energy 2017;112:124–42.
[12] Li T, Rabuni MF, Kleiminger L, Wang B, Kelsall GH, Hartley UW, et al. A highly-robust solid oxide fuel cell (SOFC): simultaneous greenhouse gas treatment and clean energy generation. Energy Environ Sci 2016;9:3682–6.
[13] Doherty W, Reynolds A, Kennedy D. Process simulation of biomass gasification integrated with a solid oxide fuel cell stack. J Power Sources 2015;277:292–303.
[14] Tan L, Dong X, Gong Z, Wang M. Investigation on performance of an integrated SOFC-GE-KC power generation system using gaseous fuel from biomass gasification. Renew Energy 2017;107:448–61.
[15] Panopoulos KD, Fryda LE, Karl J, Poulou S, Kakaras E. High temperature solid oxide fuel cell integrated with novel allothermal biomass gasification: Part I: modelling and feasibility study. J Power Sources 2006;159:570–85.
[16] Perna A, Minutillo M, Jannelli E, Cigolotti V, Nam SW, Yoon KJ. Performance assessment of a hybrid SOFC/MGT cogeneration power plant fed by syngas from a biomass down-draft gasifier. Appl Energy 2018;227:80–91.
[17] Shu G, Liang Y, Wei H, Tian H, Zhao J, Liu L. A review of waste heat recovery on two-stroke IC engine aboard ships. Renew Sustain Energy Rev 2013;19:385–401.
[18] Xu B, Rathod D, Yebi A, Filipi Z, Onori S, Hoffman M. A comprehensive review of organic rankine cycle waste heat recovery systems in heavy-duty diesel engine applications. Renew Sustain Energy Rev 2019;107:145–70.
[19] Ranjbar F, Chitsaz A, Mahmoudi SMS, Khalilarya S, Rosen MA. Energy and exergy assessments of a novel trigeneration system based on a solid oxide fuel cell. Energy Convers Manag 2014;87:318–27.
[20] Oryshchyn D, Harun NF, Tucker D, Bryden KM, Shadle L. Fuel utilization effects on system efficiency in solid oxide fuel cell gas turbine hybrid systems. Appl Energy 2018;228:1953–65.
[21] Ahmadi S, Ghaebi H, Shokri A. A comprehensive thermodynamic analysis of a novel CHP system based on SOFC and APC cycles. Energy 2019;186:115899. https://doi.org/10.1016/j.energy.2019.115899.
[22] Haseli Y, Dincer I, Naterer GF. Thermodynamic analysis of a combined gas turbine power system with a solid oxide fuel cell through exergy. Thermochim Acta 2008;480:1–9.
[23] Ho T, Mao SS, Greif R. Comparison of the Organic Flash Cycle (OFC) to other advanced vapor cycles for intermediate and high temperature waste heat reclamation and solar thermal energy. Energy 2012;42:213–23.
[24] Lee HY, Park SH, Kim KH. Comparative analysis of thermodynamic performance and optimization of organic flash cycle (OFC) and organic Rankine cycle (ORC). Appl Therm Eng 2016;100:680–90.
[25] Hadelu LM, Boyaghchi FA. Exergoeconomic and exergoenvironmental analyses and optimization of different ejector based two stage expander-organic flash cycles fuelled by solar energy. Energy Convers Manag 2020;216:112943.
[26] Wu C, Xu X, Li Q, Li X, Liu L, Liu C. Performance assessment and optimization of a novel geothermal combined cooling and power system integrating an organic flash cycle with an ammonia-water absorption refrigeration cycle. Energy Convers Manag n.d.;227:113562.
[27] Klein SA, Alvarado FL. Engineering equation solver, vol. 1. Madison, WI: F-Chart Software; 2002.
[28] Rostamzadeh H, Ebadollahi M, Ghaebi H, Shokri A. Comparative study of two novel micro-CCHP systems based on organic Rankine cycle and Kalina cycle. Energy Convers Manag 2019. https://doi.org/10.1016/j.enconman.2019.01.003.
[29] Parikhani T, Jannatkhah J, Shokri A, Ghaebi H. Thermodynamic analysis and optimization of a novel power generation system based on modified Kalina and GT-MHR cycles. Energy Convers Manag 2019;196. https://doi.org/10.1016/j.enconman.2019.06.018.
[30] Behzadi A, Houshfar E, Gholamian E, Ashjaee M, Habibollahzade A. Multi-criteria optimization and comparative performance analysis of a power plant fed by municipal solid waste using a gasifier or digester. Energy Convers Manag 2018;171:863–78.
[31] Mehrabadi ZK, Boyaghchi FA. Thermodynamic, economic and environmental impact studies on various distillation units integrated with gasification-based multi-generation system: comparative study and optimization. J Clean Prod 2019;241:118333.
[32] Boyaghchi FA, Chavoshi M, Sabeti V. Multi-generation system incorporated with PEM electrolyzer and dual ORC based on biomass gasification waste heat recovery: exergetic, economic and environmental impact optimizations. Energy 2018;145:38–51.
[33] Moran MJ, Shapiro HN, Boettner DD, Bailey MB. Fundamentals of engineering thermodynamics. John Wiley & Sons; 2010.
[34] Gholamian E, Zare V, Mousavi SM. Integration of biomass gasification with a solid oxide fuel cell in a combined cooling, heating and power system: a thermodynamic and environmental analysis. Int J Hydrogen Energy 2016;41:20396–406.
[35] Jia J, Li Q, Luo M, Wei L, Abudula A. Effects of gas recycle on performance of solid oxide fuel cell power systems. Energy 2011;36:1068–75.
[36] Zhao H, Jiang T, Hou H. Performance analysis of the SOFC–CCHP system based on H2O/Li–Br absorption refrigeration cycle fueled by coke oven gas. Energy 2015;91:983–93.
[37] Kuchonthara P, Bhattacharya S, Tsutsumi A. Energy recuperation in solid oxide fuel cell (SOFC) and gas turbine (GT) combined system. J Power Sources 2003;117:7–13.
[38] Dincer I, Rosen MA, Ahmadi P. Optimization of energy systems. Wiley Online Library; 2017.
[39] Behzadi A, Gholamian E, Houshfar E, Habibollahzade A. Multi-objective optimization and exergoeconomic analysis of waste heat recovery from Tehran's waste-to-energy plant integrated with an ORC unit. Energy 2018;160:1055–68.
[40] Bejan A, Tsatsaronis G, Moran MJ. Thermal design and optimization. John Wiley & Sons; 1995.
[41] Behzadi A, Gholamian E, Ahmadi P, Habibollahzade A, Ashjaee M. Energy, exergy and exergoeconomic (3E) analyses and multi-objective optimization of a solar and geothermal based integrated energy system. Appl Therm Eng 2018;143:1011–22.
[42] Tao G, Armstrong T, Virkar A. Intermediate temperature solid oxide fuel cell (IT-SOFC) research and development activities at MSRI. Ninet. Annu. ACERC&ICES Conf. 2005.
[43] Gholamian E, Mahmoudi SMS, Zare V. Proposal, exergy analysis and optimization of a new biomass-based cogeneration system. Appl Therm Eng 2016;93:223–35.
[44] Zainal ZA, Ali R, Lean CH, Seetharamu KN. Prediction of performance of a downdraft gasifier using equilibrium modeling for different biomass materials. Energy Convers Manag 2001;42:1499–515.
[45] Alauddin ZAZ. Performance and characteristics of a biomass gasifier system. Ph.D. thesis. College of Cardiff, UK: University of Wales; 1996.